2024 IEEE International Conference on Robotics and Automation (ICRA 2024)
May 13-17, 2024. Yokohama, Japan

Transparency Control of a 1-DoF Knee Exoskeleton via Human-in-the-Loop Velocity Optimisation

Lukas Cha[1], Annika Guez[2], Chih-Yu Chen[1], Sion Kim[2], Zhenhua Yu[2], Bo Xiao[2] and Ravi Vaidyanathan[2]

***Abstract*—Rehabilitative robotics, particularly lower-limb exoskeletons (LLEs), have gained increasing importance in aiding patients regain ambulatory functions. One of the challenges in making these systems effective is the implementation of an assist-as-needed (AAN) control strategy that intervenes only when the patient deviates from the correct movement pattern. Equally crucial is the need for the LLE to exhibit "transparency" — minimising its interaction forces with the wearer to feel as natural as possible. This paper introduces a novel approach to transparency control based on a human-in-the-loop velocity optimisation framework. The proposed method employs torque data captured from past steps through a Series Elastic Actuator (SEA) to approximate the wearer's intended future movements and computes a corresponding transparent velocity trajectory. The velocity commands are complemented by an Adaptive Frequency Oscillator (AFO) based position controller that leverages the periodic nature of human gait and is modified with a force sensor for increased reactiveness to human gait variations. This approach is experimentally evaluated against a standard zero-torque controller with a stationary single-degree-of-freedom knee exoskeleton test platform in a proof-of-concept study. Preliminary results indicate that combining adaptive oscillators with interaction force sensing can improve transparency compared to the conventional zero-torque controller, using force readings for position control and torque measurements for velocity optimisation and control.**

***Index Terms*—exoskeleton, transparency, control, human-in-the-loop, series-elastic-actuator, optimisation**

I. Introduction

In addition to traditional physiotherapeutic approaches, rehabilitative robotics are increasingly used to help patients regain their ability to move [1], [2]. In the context of recovering ambulatory ability, lower-limb exoskeletons (LLEs) are specifically of interest [3]. For effective rehabilitation, patient participation is crucial; an assist-as-needed (AAN) control strategy ensures this by only providing assistive torque when the user deviates from the desired trajectory [3], [4]. During the instances where no corrective torque is applied, the LLE needs to minimise the effect of its inertia and friction on the wearer [5]. Thus, it needs to feel *transparent* to the wearer, calling for the need of a *transparency control* mode as the baseline control mode for an effective AAN approach.

Transparency is generally achieved when the interaction forces between the exoskeleton structure and the human wearer are as close to zero as possible. Whilst these are inevitable in practice due to physical interactions (gravity, shear forces, etc.) and misalignment of the human and exoskeleton axis [6], [7], motion-based forces can be minimised with a suitable control strategy, by matching the exoskeleton movement with the human movement such that there is a full kinematic synchronisation [8]. In particular, by matching the exoskeleton velocity to the human limb velocity [9], significant amounts of tangential interaction forces in the direction of movement due to collision can be avoided.

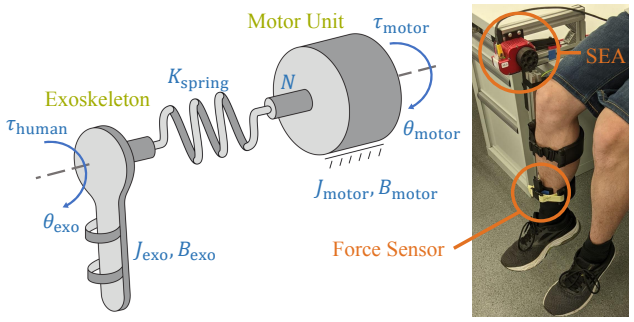

Fig. 1: Schematic depicting a simplified series-elastic-actuator with the single degree-of-freedom knee exoskeleton (left) and the experimental setup (right).

Apart from hardware side developments that aim to improve transparency with novel actuators [10], [11], many of the software side transparency approaches can be categorised into model-free and model-based control approaches. An example model-free approach utilises machine learning algorithms to train the controller to be transparent. Chen et al. [8] employ a kernel-based method to estimate the activation level of a muscle model with electromyography (EMG) for force-position control. A finite state machine based transparency approach is improved by smoothly blending the transitions using collected user data and a customised blending is computed via linear regression [12] or neural networks [13]. These approaches, however, have to be personalised to individual users and thus involve increased preparation time and effort for use.

Another popular model-free approach towards transparency uses Adaptive Frequency Oscillators (AFOs) [14], which function like Central Pattern Generator models modified with the ability to adapt to an external input [15]. This feature allow the AFOs to take advantage of the cyclic nature of human gait by matching the oscillator frequencies to the human movement and thus provide accurate estimates of the gait phase for control [16]–[18]. Whilst AFOs can conflict with rigid proportional–integral–derivative (PID) control, as the latter suppresses voluntary human movements, the integration

[1]TUM School of Engineering and Design, Technical University of Munich, Munich, Germany
[2]Department of Mechanical Engineering, Imperial College London, London, United Kingdom

of force sensors in our proposed approach enhances the AFOs' responsiveness to changes in human intentions and thus its compatibility with such a conventional position controller.

Model-based methods rely on the dynamics modelling of the exoskeleton system to compute the interaction torque for compensation [19], for use in combination with an inertial measurement unit (IMU) for an acceleration-based transparency control [20] or as part of a Markovian approach to estimate the current gait cycle phase as states in a Markov chain [21]. Our proposed method includes dynamics modelling with the goal of relating the torques sensed by the Series Elastic Actuator (SEA) to the torques required to move the exoskeleton structure.

Using these two torque values, one can therefore give the controller the ability to predict the future human intended movement based on past torque measurements. Our contribution in this paper is a transparency control approach based on *human-in-the-loop* optimisation that uses the SEA measured torque of past steps in order to predicatively compute a transparent velocity trajectory for future steps. This is complemented by an AFO-based position computation that integrates interaction force measurements. As it uses human-in-the-loop optimisation to compute a transparent velocity trajectory, it is termed the Velocity-Optimising Transparency Controller (VOTC).

II. Methods

The proposed controller computes both desired position and velocity trajectories such that, when executed in unison, a high level of exoskeleton movement transparency is achieved within the physical limit. The control signals for position and velocity are processed through a cascaded PID controller as shown on the right in Fig. 2, which then calculates a Pulse-width modulation (PWM) signal for the motor as a balanced compromise between the two. The proposed controller is shown on the left in Fig. 2 and the below sections detail the computations involved for the position and velocity signals.

A. Position Computation

The position computation leverages the periodicity of human gait, which implies that consecutive steps will tend to have relatively similar trajectory profiles [17]. An AFO can therefore be utilised to memorise the gait pattern of past steps [14]. While the AFO is capable of successfully exploiting the cyclic nature of gait, it struggles to register sudden changes in gait pattern or significant variations within a step. To remedy this, a force sensor was added to modify the AFO output by monitoring the human-exoskeleton interaction forces for the PID to adapt the provided torque accordingly.

1) Adaptive Frequency Oscillators: AFOs are a system of first order Ordinary Differential Equations (ODEs) that are capable of reconstructing any periodic input signal, first explored for engineering applications by Righetti et al. [14]. They proposed a structure featuring a pool of oscillators in parallel, with each oscillator tasked to learn one frequency component of the input signal. For the knee angle trajectory during walking that is nearly periodic, the frequency components are thus multiples of a base frequency. The following equations describe the structure of such a pool of adaptive oscillators [16]:

$$\dot{\phi}_i(t) = i\omega(t) + \nu_\phi E(t)\cos\phi_i(t) \tag{1}$$

$$\dot{\omega}(t) = \nu_\omega E(t)\cos\phi_1(t) \tag{2}$$

$$\dot{\alpha}_i(t) = \eta E(t)\sin\phi_i(t) \tag{3}$$

$$E(t) = \theta(t) - \theta_{\text{AFO}}(t) \tag{4}$$

$$\theta_{\text{AFO}}(t) = \alpha_0 + \sum_{i=1}^{k} \alpha_i(t)\sin\phi_i(t) \tag{5}$$

with $i \in [0, k]$ for k oscillators in parallel. Equation (1) is the phase oscillator with $\phi_i(t)$ as the oscillator phase and $\omega(t)$ the base frequency. For the phase oscillator to learn the frequency of the teaching signal $E(t)$, the dynamics of $\omega(t)$ as an integrator of the phase update is set as in (2). With these dynamics, the phase oscillator is an adaptive oscillator that can adapt its frequency $\omega(t)$ to the teaching signal frequency. The AFO output $\theta_{\text{AFO}}(t)$ can then be formulated using (5), which is a sum of sinusoids with a constant α_0 offset. After a period of learning from the input signal $\theta(t)$, the sinusoid weights $\alpha_i(t)$ then converge such that $\theta_{\text{AFO}}(t)$ estimates $\theta(t)$. This is achieved by defining the teaching signal $E(t)$ and the dynamics of weights $\alpha_i(t)$ as in (4) and (3). For our AFO implementation, we set the number of oscillators to be $k = 5$ and the learning parameters that define the dynamics of the system to be $\nu_\omega = 2.22$, $\nu_\phi = 7.33$ and $\eta = 0.67$. To generate a gait cycle percentage (GC%) value that resets every 2π, $\mod(\phi_1(t), 2\pi)$ is computed using the phase of the base harmonic $i = 1$.

2) Force Sensor Position Modification: To increase the responsiveness of the AFO to in-step variations present in human gait, a force sensor is added to allow for an instantaneous correction of the outputted $\theta_{\text{AFO}}(t)$ position command. The force sensor used is a DF9-40 force-sensitive resistor that is capable of registering normal forces up to 20 N (Precision: $\pm 2.5\%$, Repeatability: $\pm 5.8\%$). To account for nonlinearities of the sensor, the mapping of the voltage values read by an Arduino Uno to the applied force values was experimentally verified with weights and a linearisation around the operation point is used for the control task. The force sensor is enclosed in a 3D printed casing that focuses the pressure point and is attached to the lower brace of the single degree-of-freedom (DoF) knee exoskeleton as shown on the right of Fig. 1. The encased sensor is placed in-between the strap and the shin bone where, unlike for muscles, there is no possible deformation, and the registered force therefore corresponds to the normal interaction forces at that contact point. The modification made to the AFO output therefore resulted in an additional term with a manually tuned gain $K = 0.12$:

$$\theta_{\text{AFO,mod}}(t) = \theta_{\text{AFO}}(t) + K \cdot F_{\text{interaction}}(t) \tag{6}$$

Here, $F_{\text{interaction}}(t)$ is the interaction force at the contact point, which is computed as a relative value to the baseline

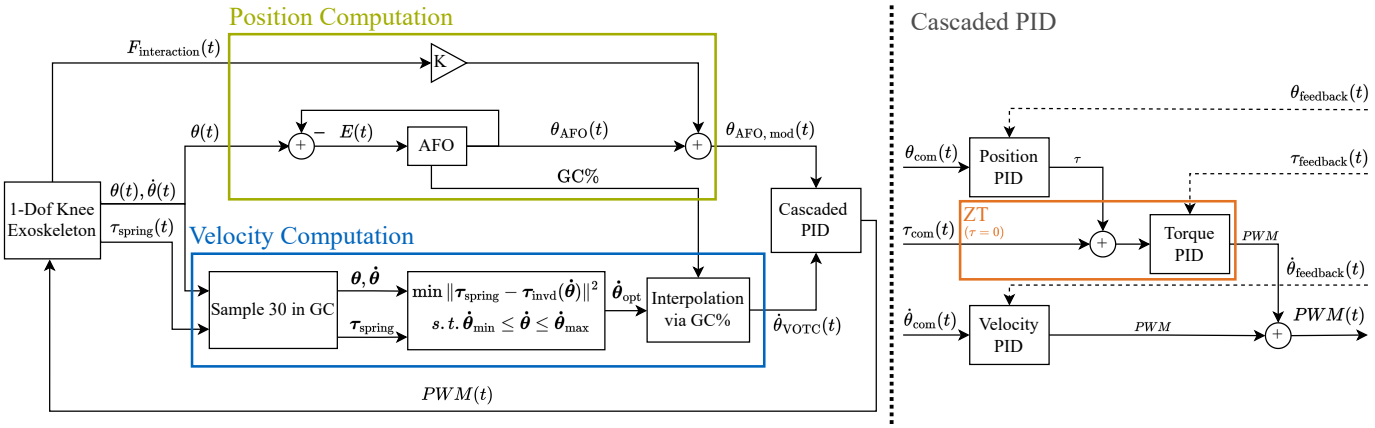

Fig. 2: Block diagram showing the VOTC control framework that includes the AFOs for the position computation and the velocity optimisation for the velocity computation (left) and the cascaded PID [22] with the active section during zero-torque (ZT) operation marked in orange (right).

contact force measured when the human-exoskeleton system is stationary. This baseline contact force value is set as the leg is initially strapped in and is then used as the operation point for the linearisation of the voltage-force mapping. $F_{\text{interaction}}(t)$ therefore corresponds to the deviation from this value in both directions, yielding both positive and negative interaction force outputs as the human leg moves against and away from the force sensor. The AFO's capacity to track the angle input signal is unaffected by the force term, shown in Fig. 3.

B. Velocity Computation

To compute a movement-transparent velocity trajectory for the next movement cycle, the proposed optimisation algorithm uses the measured torque profile of the previous cycle to estimate the trend of the movement i.e. infer the intentions of the wearer from their interaction with the SEA. The torque measured by the SEA spring consists of both the externally applied torques and the motor torques required to move the load with its current kinematics. In this case, the externally applied torques are the human interaction torques τ_{human} and the load is the exoskeleton structure.

1) Dynamics Modelling: The following equations describe the dynamics of the stationary knee exoskeleton test rig on the motor side and on the exoskeleton structure side, derived by considering the free body diagrams that split the schematic drawing in Fig. 1 at the position of the torsional spring with the gear ratio N embedded in the depicted motor unit [23]:

$$J_{\text{motor}}\ddot{\theta}_{\text{motor}} + B_{\text{motor}}\dot{\theta}_{\text{motor}} = \tau_{\text{motor}} - \frac{1}{N}\tau_{\text{spring}} \tag{7}$$

$$J_{\text{exo}}\ddot{\theta}_{\text{exo}} + B_{\text{exo}}\dot{\theta}_{\text{exo}} + \tau_{\text{exo,g}}\sin(\theta_{\text{exo}}) = \tau_{\text{spring}} + \tau_{\text{human}} \tag{8}$$

Here, $\tau_{\text{exo,g}}$ in (8) is the lumped gravitational torque induced by the exoskeleton structure. Note that the inertia, friction and gravitational terms with the parameters J_{exo}, B_{exo} and $\tau_{\text{exo,g}}$ only consider the exoskeleton structure and exclude the human leg. This is because, in this dynamics modelling, the exoskeleton structure is viewed as its own separate system and the only interaction from the human is via the human's contributed interaction torque τ_{human}. The system parameters for the LLE were computed by collecting kinematic data and the SEA outputted τ_{spring} for executed reference sinusoidal trajectories of varying frequencies. In scenarios without human involvement, τ_{human} is zero and (8) can be used for least squares fitting to identify the parameters ($J_{\text{exo}} = 0.0377$ kg·m^2, $B_{\text{exo}} = 0.0207$ Nm·s·rad^{-1}, $\tau_{\text{exo,g}} = 1.7536$ Nm) [24].

The torque τ_{spring} measured by the SEA is computed from the relative rotational deflections between motor-side shaft and output-side shaft measured by absolute encoders on each respective side, described by the equations:

$$\tau_{\text{spring}} = K_{\text{spring}}\theta_{\text{spring}} \tag{9}$$

$$\theta_{\text{spring}} = \frac{1}{N}\theta_{\text{motor}} - \theta_{\text{exo}} \tag{10}$$

Equation (8) describes the relationship between the SEA measured torque τ_{spring}, the human interaction torque τ_{human} and the torque required to move the exoskeleton structure with the kinematics ($\ddot{\theta}_{\text{exo}}$, $\dot{\theta}_{\text{exo}}$, θ_{exo}). To achieve movement transparency, the idea is thus to minimise the term τ_{human} in (8). Mathematically, to have a minimal absolute value for τ_{human}, the other remaining terms should match:

$$|\tau_{\text{human}}| = \left|J_{\text{exo}}\ddot{\theta}_{\text{exo}} + B_{\text{exo}}\dot{\theta}_{\text{exo}} + \tau_{\text{exo,g}}\sin(\theta_{\text{exo}}) - \tau_{\text{spring}}\right| \tag{11}$$

Since the terms involving ($\ddot{\theta}_{\text{exo}}$, $\dot{\theta}_{\text{exo}}$, θ_{exo}) compose the inverse dynamics equation that computes the torque required to move the exoskeleton with these kinematics, they are denoted with:

$$\tau_{\text{invd}}(\ddot{\theta}_{\text{exo}}, \dot{\theta}_{\text{exo}}, \theta_{\text{exo}}) = J_{\text{exo}}\ddot{\theta}_{\text{exo}} + B_{\text{exo}}\dot{\theta}_{\text{exo}} + \tau_{\text{exo,g}}\sin(\theta_{\text{exo}}) \tag{12}$$

Therefore, to have a minimal human involvement in the movement of the exoskeleton structure, the kinematics of the exoskeleton should be adjusted such that the term τ_{invd} matches the measured τ_{spring}, minimising both sides of (11) and thus indirectly minimising τ_{human}. With a decreased τ_{human}, the decreased involvement of the human in the movement of

the exoskeleton implies that the exoskeleton dynamics and human leg dynamics are as decoupled as possible, increasing movement transparency.

2) Constrained Least Squares Optimisation: To generate movement-transparent velocities, equation (11) is used as the basis of the cost function. Since (11) only considers one point in time and the aim is to compute an optimal velocity trajectory over the next cycle, each cycle is discretised into $n = 30$ elements and the difference between the optimisation variable τ_{invd}, and the measured τ_{spring} value is minimised at each time point. The number of discretisation points was chosen to be 30 as a good compromise between computational cost and accuracy. The optimisation procedure for a single cycle can be viewed as a curve fitting problem where the n element curve $\boldsymbol{\tau}_{\text{invd}}$ should match the n element curve $\boldsymbol{\tau}_{\text{spring}}$ obtained from measurements. The constrained nonlinear least squares optimisation problem can be formulated as follows with θ_{exo} set to θ henceforth for brevity:

$$\begin{aligned} \min_{\dot{\boldsymbol{\theta}}} \quad & \left\| \boldsymbol{\tau}_{\text{spring}} - \boldsymbol{\tau}_{\text{invd}}(\dot{\boldsymbol{\theta}}) \right\|^2 \\ s.t. \quad & \dot{\boldsymbol{\theta}}_{\min} \leq \dot{\boldsymbol{\theta}} \leq \dot{\boldsymbol{\theta}}_{\max} \end{aligned} \tag{13}$$

In practice, the implementation is done as follows: using the GC% outputted by the AFO as shown in Fig. 3, the beginning of a new cycle can be detected in real-time at the reset point of the phase curve. For the optimisaton performed once at this transition point between cycles, the n element torque curve $\boldsymbol{\tau}_{\text{spring}}$ from SEA torque data sampled in regular phase intervals across the last cycle is available. Additionally, the positions $\boldsymbol{\theta}_{\text{pc}}$ and velocities $\dot{\boldsymbol{\theta}}_{\text{pc}}$ from the past cycle are available from the same regular sampling. Since the optimisation problem in equation (13) only has the velocities $\dot{\boldsymbol{\theta}}$ as the optimisation variable, the positions $\boldsymbol{\theta}$ is obtained from integration of $\dot{\boldsymbol{\theta}}$ using the constant last value of the measured $\boldsymbol{\theta}_{\text{pc}}$. The accelerations $\ddot{\boldsymbol{\theta}}$ are obtained via numerical differentiation. This yields $\boldsymbol{\tau}_{\text{invd}}(\dot{\boldsymbol{\theta}})$ as a function solely dependent on the optimisation variable $\dot{\boldsymbol{\theta}}$ and can be used for optimisation function evaluations.

To compute the optimal $\dot{\boldsymbol{\theta}}_{\text{opt}}$, the measured $\dot{\boldsymbol{\theta}}_{\text{pc}}$ from the past cycle is set as the initial guess $\dot{\boldsymbol{\theta}}_{\text{init}}$. Upper and lower bounds are defined as a tube of radius 0.7 rad/s around the initial guess. This is an important safety measure that guarantees that the optimised velocity trajectory result can only change within safe limits from one cycle to the next. The upper plot in Fig. 4 shows an example of such an optimisation for one cycle where the torque curve begins at $\boldsymbol{\tau}_{\text{invd,init}} = \boldsymbol{\tau}_{\text{invd}}(\dot{\boldsymbol{\theta}}_{\text{init}})$ and ends at $\boldsymbol{\tau}_{\text{invd,opt}} = \boldsymbol{\tau}_{\text{invd}}(\dot{\boldsymbol{\theta}}_{\text{opt}})$ after the optimisation converges to a solution. The respective initial and optimised curves for the velocity are shown in the lower plot. The optimised velocity curve is then interpolated to 1000 points and using the GC% from the AFOs, a velocity command $\dot{\theta}_{\text{VOTC}}(t)$ synchronised with the current position command is generated.

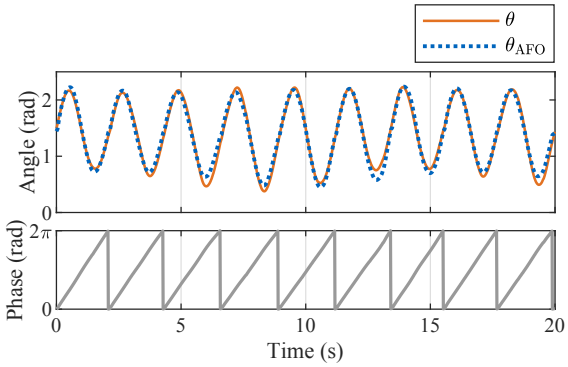

Fig. 3: The upper figure shows how the AFO output θ_{AFO} is capable of tracking the input angle θ with the force sensor position modification active. The lower figure shows the GC% curve outputted by the AFO.

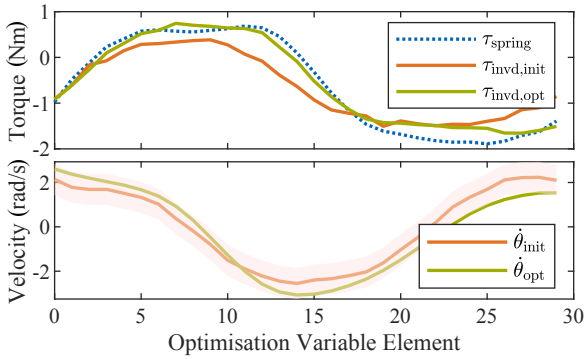

Fig. 4: The upper figure shows the result of the optimisation process for the torques, which translates into an optimisation of the velocity curves as seen in the lower figure, where the pink shade represents the allowed region defined by the upper and lower bounds.

III. Experiment

To evaluate the VOTC method against the zero-torque controller, five leg extension experiments were performed at two different frequencies and amplitudes for a duration of 60 s, as detailed in Table I. Here, the zero-torque controller is simply the cascaded PID controller shown in Fig. 2 with the position and velocity PIDs inactive and $\tau_{\text{com}}(t)$ set to zero. In the four experiments termed *Steady State*, the leg was periodically extended from a natural resting position to the specified maximum amplitude and at the specified frequency, which was maintained with a metronome. In the experiment termed *Dynamic*, the leg was extended twice to the lower amplitude and then extended twice to the higher amplitude at the lower frequency, with one transitional amplitude extension allowed in between. The experiments were each repeated twice with a single test subject. Suitable actuator limits were set to ensure user safety. A video of the experiment is given as supplementary material: https://youtu.be/lC9OYfI626I.

In order to initiate the AFO such that it is trained with the correct frequency to provide the correct phase percentage and θ_{AFO} output immediately, all the VOTC experiments included an initial 15 s of running the exoskeleton at the desired sinusoidal leg extension trajectory at the respective frequency and amplitude. This adaptation time procedure during evaluation is also seen with other AFO-based methods [17], [18].

The controller on the host PC was run at 75 Hz with the MATLAB (Mathworks, USA) API for the HEBI X8-9 actuator (HEBI Robotics, USA) with the frequency chosen to accommodate the MATLAB-Arduino communication time for the force sensor. The computation runs on a 64-bit Windows 11 operated computer with 32 GB RAM and with a 14-core Intel i9-13900H CPU running at 2.6 GHz. MATLAB's *lsqnonlin* routine with the *trust-region-reflective* algorithm was used for the optimisation.

TABLE I: Frequency and amplitudes for the five different leg extension experiments.

Experiment	Frequency (Hz)	Amplitude (deg)
Steady State 1	0.45	40
Steady State 2	0.45	60
Steady State 3	0.60	40
Steady State 4	0.60	60
Dynamic	0.45	40/60

IV. Preliminary Results and Discussion

A. Exo-Human Kinematic Synchronisation

Figure 6 shows the position and velocity tracking performances of the VOTC method for a 20 s long post initial phase window in the *Steady State 2* and the *Dynamic* experiment as defined in Table I. Overall, the VOTC appears to successfully track the user's motion, with the predicted velocity for both the steady state and dynamic conditions maintaining periodicity, despite experiencing slight discontinuities at the peaks, i.e. the transition point between cycles in the commanded velocity curve. This is due to the absence of continuity and smoothness constraints in the current least squares optimisation problem formulation. The velocity tracking errors from overshoots and undershoots of the desired velocity curve could also be due to its computation with optimisation relying on torque data from the previous cycle, which can only provide an approximate indication for human movement trends. In addition, the inherent compliant nature of the SEA's internal spring presents a barrier to very precise tracking, but this can aid transparent behaviour. With the commanded angles in Fig. 6, there is generally close tracking for both the steady state and dynamic experiment except at the peaks. Once more, the tracking error could similarly be due the inherent compliance induced by the spring in the SEA, which tends to dampen motion peaks to ensure a smooth output and user safety. In the context of movement transparency control, these behaviours suggest that the commanded signals closely align with user's intended movement, therefore indicating minimal collision between the human and the exoskeleton. Such collisions would have resulted in spurious sections of poor tracking, as θ_{exe} and $\dot{\theta}_{\text{exe}}$ of the exoskeleton would be forced to deviate from their desired curves by human interaction, which was not observed with the VOTC method.

B. Interaction Force Evaluation

As interaction forces are the most direct measure for transparency [12], they are evaluated to benchmark the VOTC method against the conventional zero-torque controller. The three metrics of *maximum amplitude*, *Root Mean Squared (RMS) amplitude* and *mean power* are chosen as the comparative metrics for the interaction forces. The bar plots in Fig. 5 show these three metrics for the experiments detailed in Table I. It can be observed that the RMS amplitudes and the mean power metrics for the interaction force are lower for the VOTC method compared the zero-torque controller for all experiments. However, the maximum amplitude registered for the interaction forces is higher for the VOTC method across all experiments. This trend is summarised in Table II, where the metric values are averaged for the steady state experiments and shown for the dynamic experiment.

An example of this overall trend is shown in the interaction force plots for two individual experiments. Fig. 7 shows the interaction forces measured for the initial 20 s of the *Steady State 2* experiment and the *Dynamic* experiment, comparing the VOTC against the zero-torque controller. For the steady state experiment, the VOTC induces lower interaction forces but with higher variation across different movement frequencies and amplitudes, as seen in the lower RMS amplitude and mean power averages but higher standard deviations in Table II. The same pattern of lower average values can be observed for the dynamic experiment. This result is expected if the computed desired position and velocity signals agree with the human intended movement, as the VOTC method tracks a trajectory as opposed to being purely reactionary like the zero-torque controller. As the latter controller can only react to momentarily sensed torques, the human is in effect always pulling the exoskeleton with the leg movement, incurring higher interaction forces.

Note, however, that slight vibrations can be observed at the transition points between cycles in Fig. 7. This is due to the velocity command discontinuities as seen in Fig. 6. Future work should therefore investigate suitable optimisation constraints that ensure continuity without deteriorating the movement transparent character of the solution. Additionally, a large spike in interaction force can be observed for the VOTC method at the beginning, as marked by the yellow rectangle in Fig. 7. This phenomenon is observed for all VOTC experiments and is reflected in the higher maximum amplitudes in Table II. This is caused by the first MATLAB *lsqnonlin* run time of 0.568 ± 0.025 s that is significantly longer than the subsequent run times, due to the internal caching system that optimises computation times for subsequent runs. The first optimisation thus delays the control loop for this optimisation time and following optimisations have more expected computation times averaging 0.046 ± 0.022 s for 35.711 ± 9.735 iterations to converge to a local minimum. Future work should

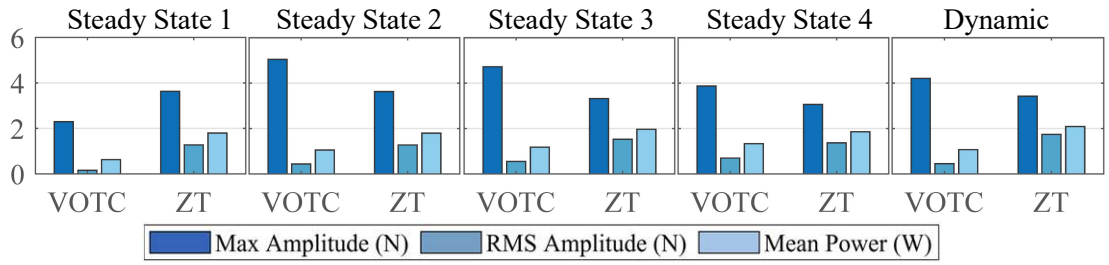

Fig. 5: Bar plots showing the interaction force metric values for the experiments detailed in Table I. ZT denotes zero-torque.

aim to resolve this issue by moving the computation to a faster C++ optimisation and control framework that is more real-time capable.

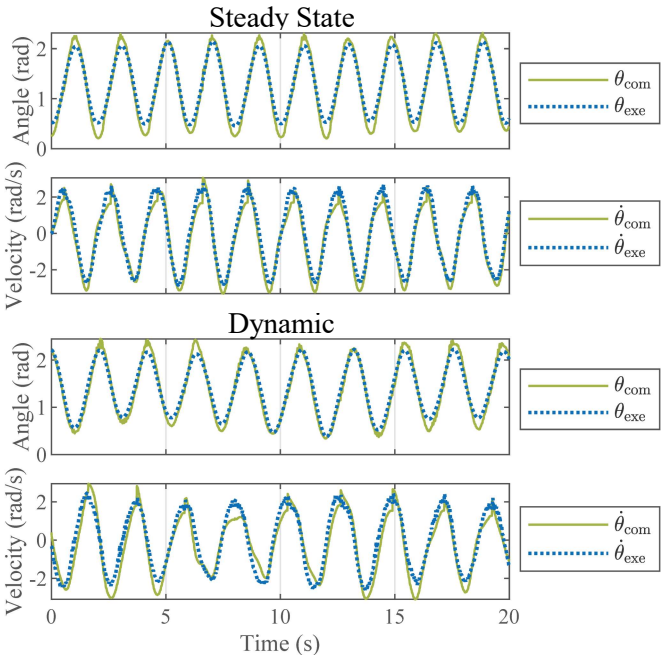

Fig. 6: Figures showing the position and velocity tracking (commanded and executed values) of the VOTC method compared to the zero-torque controller in the *Steady State 2* experiment and the *Dynamic* experiment from Table I.

TABLE II: Interaction force metric values for VOTC and the zero-torque controller averaged across all steady state experiments and shown for the dynamic experiment.

	Maximum Amplitude (N)	**RMS Amplitude (N)**	**Mean Power (W)**
Zero-Torque Overall Steady State	3.37 ±0.24	1.31 ±0.19	1.82 ±0.13
VOTC Overall Steady State	3.98 ±1.23	0.46 ±0.23	1.05 ±0.30
Zero-Torque Dynamic	3.79	0.88	1.44
VOTC Dynamic	4.21	0.45	1.07

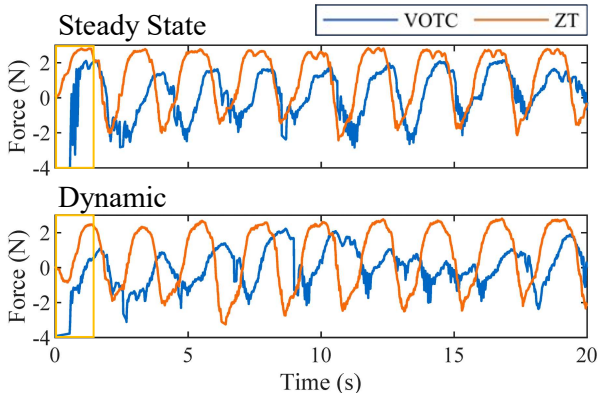

Fig. 7: Figures showing the interaction forces for the two methods measured at the location of the force sensor for the initial 20 s of the *Steady State 2* experiment and the *Dynamic* experiment. ZT denotes zero-torque.

V. Conclusion

We propose the VOTC, a method that employs AFOs with interaction force sensing for position computation, combined with velocity optimisation from torque measurements. An experiment was conducted to compare the movement transparency performance of the VOTC method against a conventional zero-torque controller in this proof-of-concept study. The preliminary results indicate that the VOTC method is able to achieve lower interaction forces for the same movements performed while wearing the exoskeleton. A limitation is that, as with any method utilising AFOs, the VOTC method is only applicable to approximately periodic movements, thus it would have to be used in combination with other control strategies e.g. the zero-torque controller to accommodate a start-stop gait pattern. However, the dynamics modelling for the velocity optimisation only involves the exoskeleton dynamics, therefore the controller does not have to be individualised to different users in contrast to methods that require human dynamics modelling. Future works should focus on extending the dynamics modelling and control framework to LLEs with higher DoFs. As our VOTC framework computes explicit desired position and velocity signals unlike the zero-torque controller, there is potential for modification of the method to achieve AAN functionality e.g. by including the force sensor data in the optimisation framework.

REFERENCES

[1] L. E. Kahn, P. S. Lum, W. Z. Rymer, and D. J. Reinkensmeyer, "Robot-assisted movement training for the stroke-impaired arm: Does it matter what the robot does?" *Journal of rehabilitation research and development*, vol. 43, no. 5, pp. 619–630, 2014.

[2] W. H. Chang and Y.-H. Kim, "Robot-assisted therapy in stroke rehabilitation," *Journal of stroke*, vol. 15, no. 3, p. 174, 2013.

[3] R. Baud, A. R. Manzoori, A. Ijspeert, and M. Bouri, "Review of control strategies for lower-limb exoskeletons to assist gait," *Journal of NeuroEngineering and Rehabilitation*, vol. 18, no. 1, pp. 1–34, 2021.

[4] S. K. Banala, S. H. Kim, S. K. Agrawal, and J. P. Scholz, "Robot assisted gait training with active leg exoskeleton (alex)," *IEEE transactions on neural systems and rehabilitation engineering*, vol. 17, no. 1, pp. 2–8, 2008.

[5] G. Aguirre-Ollinger, J. E. Colgate, M. A. Peshkin, and A. Goswami, "Inertia compensation control of a one-degree-of-freedom exoskeleton for lower-limb assistance: Initial experiments," *IEEE transactions on neural systems and rehabilitation engineering*, vol. 20, no. 1, pp. 68–77, 2012.

[6] A. Bull and A. Amis, "Knee joint motion: description and measurement," *Proceedings of the Institution of Mechanical Engineers, Part H: Journal of Engineering in Medicine*, vol. 212, no. 5, pp. 357–372, 1998.

[7] D. Zanotto, Y. Akiyama, P. Stegall, and S. K. Agrawal, "Knee joint misalignment in exoskeletons for the lower extremities: Effects on user's gait," *IEEE Transactions on Robotics*, vol. 31, no. 4, pp. 978–987, 2015.

[8] X. Chen, Y. Zeng, and Y. Yin, "Improving the Transparency of an Exoskeleton Knee Joint Based on the Understanding of Motor Intent Using Energy Kernel Method of EMG," *IEEE Transactions on Neural Systems and Rehabilitation Engineering*, vol. 25, no. 6, pp. 577–588, Jun. 2017, conference Name: IEEE Transactions on Neural Systems and Rehabilitation Engineering.

[9] R. M. Andrade, S. Sapienza, and P. Bonato, "Development of a "transparent operation mode" for a lower-limb exoskeleton designed for children with cerebral palsy," in *2019 IEEE 16th International Conference on Rehabilitation Robotics (ICORR)*, Jun. 2019, pp. 512–517, iSSN: 1945-7901.

[10] Y. Qian, S. Han, Y. Wang, H. Yu, and C. Fu, "Toward Improving Actuation Transparency and Safety of a Hip Exoskeleton With a Novel Nonlinear Series Elastic Actuator," *IEEE/ASME Transactions on Mechatronics*, vol. 28, no. 1, pp. 417–428, Feb. 2023, conference Name: IEEE/ASME Transactions on Mechatronics.

[11] J. Song, A. Zhu, Y. Tu, X. Zhang, and G. Cao, "Novel design and control of a crank-slider series elastic actuated knee exoskeleton for compliant human–robot interaction," *IEEE/ASME Transactions on Mechatronics*, vol. 28, no. 1, pp. 531–542, 2023.

[12] C. Camardella, F. Porcini, A. Filippeschi, S. Marcheschi, M. Solazzi, and A. Frisoli, "Gait Phases Blended Control for Enhancing Transparency on Lower-Limb Exoskeletons," *IEEE Robotics and Automation Letters*, vol. 6, no. 3, pp. 5453–5460, Jul. 2021, conference Name: IEEE Robotics and Automation Letters.

[13] V. Lippi, C. Camardella, A. Filippeschi, and F. Porcini, "Identification of Gait Phases with Neural Networks for Smooth Transparent Control of a Lower Limb Exoskeleton," Jul. 2021, arXiv:2107.03746 [cs]. [Online]. Available: http://arxiv.org/abs/2107.03746

[14] L. Righetti, J. Buchli, and A. J. Ijspeert, "Dynamic Hebbian learning in adaptive frequency oscillators," *Physica D: Nonlinear Phenomena*, vol. 216, no. 2, pp. 269–281, Apr. 2006. [Online]. Available: https://www.sciencedirect.com/science/article/pii/S0167278906000819

[15] ——, "From dynamic hebbian learning for oscillators to adaptive central pattern generators," in *Proceedings of 3rd International Symposium on Adaptive Motion in Animals and Machines–AMAM 2005*, no. CONF. Verlag ISLE, Ilmenau, 2005.

[16] R. Ronsse, T. Lenzi, N. Vitiello, B. Koopman, E. van Asseldonk, S. M. M. De Rossi, J. van den Kieboom, H. van der Kooij, M. C. Carrozza, and A. J. Ijspeert, "Oscillator-based assistance of cyclical movements: model-based and model-free approaches," *Medical & Biological Engineering & Computing*, vol. 49, no. 10, pp. 1173–1185, Oct. 2011. [Online]. Available: https://doi.org/10.1007/s11517-011-0816-1

[17] W. van Dijk, H. van der Kooij, B. Koopman, E. H. F. van Asseldonk, and H. van der Kooij, "Improving the transparency of a rehabilitation robot by exploiting the cyclic behaviour of walking," in *2013 IEEE 13th International Conference on Rehabilitation Robotics (ICORR)*, Jun. 2013, pp. 1–8, iSSN: 1945-7901.

[18] Y. Zhang, K. J. Nolan, and D. Zanotto, "Oscillator-Based Transparent Control of an Active/Semiactive Ankle-Foot Orthosis," *IEEE Robotics and Automation Letters*, vol. 4, no. 2, pp. 247–253, Apr. 2019, conference Name: IEEE Robotics and Automation Letters.

[19] E. B. Küçüktabak, Y. Wen, S. J. Kim, M. Short, D. Ludvig, L. Hargrove, E. Perreault, K. Lynch, and J. Pons, "Haptic Transparency and Interaction Force Control for a Lower-Limb Exoskeleton," Jan. 2023, arXiv:2301.06244 [cs, eess]. [Online]. Available: http://arxiv.org/abs/2301.06244

[20] T. Boaventura and J. Buchli, "Acceleration-based transparency control framework for wearable robots," in *2016 IEEE/RSJ International Conference on Intelligent Robots and Systems (IROS)*. Daejeon, South Korea: IEEE, Oct. 2016, pp. 5683–5688. [Online]. Available: http://ieeexplore.ieee.org/document/7759836/

[21] F. M. Escalante, L. F. d. Santos, Y. Moreno, A. A. G. Siqueira, M. H. Terra, and T. Boaventura, "Markovian Transparency Control of an Exoskeleton Robot," *IEEE Robotics and Automation Letters*, vol. 8, no. 2, pp. 544–551, Feb. 2023, conference Name: IEEE Robotics and Automation Letters.

[22] HEBI Robotics, "Motor Control - Core Concepts," https://docs.hebi.us/core_concepts.html#motor_control, 2024, accessed: 2024-02-23.

[23] I. Kang, R. R. Peterson, K. R. Herrin, A. Mazumdar, and A. J. Young, "Design and validation of a torque-controllable series elastic actuator-based hip exoskeleton for dynamic locomotion," *Journal of Mechanisms and Robotics*, vol. 15, no. 2, p. 021007, 2023.

[24] C. Caulcrick, W. Huo, E. Franco, S. Mohammed, W. Hoult, and R. Vaidyanathan, "Model predictive control for human-centred lower limb robotic assistance," *IEEE Transactions on Medical Robotics and Bionics*, vol. 3, no. 4, pp. 980–991, 2021.